

# Robust Registration of Gaussian Mixtures for Colour Transfer

Mairéad Grogan & Rozenn Dahyot  
 School of Computer Science and Statistics  
 Trinity College Dublin, Ireland

**Abstract**—We present a flexible approach to colour transfer inspired by techniques recently proposed for shape registration. Colour distributions of the palette and target images are modelled with Gaussian Mixture Models (GMMs) that are robustly registered to infer a non linear parametric transfer function. We show experimentally that our approach compares well to current techniques both quantitatively and qualitatively. Moreover, our technique is computationally the fastest and can take efficient advantage of parallel processing architectures for recolouring images and videos. Our transfer function is parametric and hence can be stored in memory for later usage and also combined with other computed transfer functions to create interesting visual effects. Overall this paper provides a fast user friendly approach to recolouring of image and video materials.

## I. INTRODUCTION

Colour transfer refers to a set of techniques that aim to modify the colour feel of a target image or video using an exemplar colour palette provided by another image or video. Most techniques are based on the idea of warping some colour statistics from the target image colour distribution to the palette image colour distribution. The transfer (or warping) function  $\phi$ , once estimated, is then used to recolor a colour pixel value  $x$  to  $\phi(x)$ . We have recently proposed to formulate the colour transfer problem as a shape registration one, whereabout a parametric warping function  $\phi_\theta(x)$ , controlled by a latent vector  $\theta$  of parameters, is directly estimated by minimising the Euclidean  $\mathcal{L}_2$  distance between the target and palette probability density functions capturing the colour content of the palette and target images [1], [2]. This paper proposes several additional improvements. First, our framework is extended so that it can take advantage of correspondences that may be available between pixels of the target and palette image. Indeed, when considering target and palette images of the same scene, correspondences can easily be computed using registration techniques, potentially creating some outlier pairs, and our technique is shown to be robust to these occurrences. In a more general setting where the content in the palette and target images is different, user defined correspondences can also be defined to constrain the recolouring, providing some needed controls to artists manipulating images. Secondly, we explore several clustering techniques when modelling the probability density functions of the target and palette image, as well as several parametric models for the warping function  $\phi_\theta$ . Finally, recolouring using the estimated warping function  $\hat{\phi} = \hat{\phi}_\theta$  is implemented using parallel programming techniques, and our approach is shown to currently be the

fastest for recolouring. Moreover, our framework allows the user to easily mix several warping functions to create new ones, suitable for generating various spatio-temporal effects for recolouring images and videos. First we present a short review of relevant and recent colour transfer techniques (Section II), as well as techniques for shape registration that serve as a background for our colour transfer technique (Section III) which combines all the advantages of past methods while providing a computationally efficient and convenient recolouring tool for users. An exhaustive set of experiments has been carried out to assess performance against leading techniques in the field (Section IV), including computational time needed for recolouring, quantitative assessments and perceptual user studies. We show the usability of our approach for creating visual effects (Section V) and conclude (Section VI).

## II. RELATED WORKS

The body of work in recolouring is very large and the reader is referred to this recent exhaustive review by Faridul et al. [3]. We focus on presenting landmark methods (Section II-A) as well as the latest techniques in the field of colour transfer that will be used for comparison with our approach. Shape registration techniques based on Gaussian mixture models are then presented in Section II-B as background information for our technique, presented in Section III.

### A. Colour transfer techniques

Early work on colour transfer started with registering statistical moments of colour distributions (Section II-A1) using a parametric affine formulation of the transfer function  $\phi$ . This methodology soon shifted to using the optimal transport framework (Section II-A2) used in its simplest form for histogram equalisation and for correcting flicker in old (grey scale) films [4]. Optimal transport techniques use non-parametric estimates of colour distributions, and the resulting algorithms for colour corrections do not provide an explicit expression of  $\phi$  but instead an estimated correspondence  $(x, \phi(x))$  for every colour pixel  $x$ . This can be memory consuming when capturing  $\phi$  on a  $256^3$  discrete RGB colour space for instance. Alternative methods (Section II-A3) instead propose to capture colour distributions with Gaussian Mixture Models and use some correspondences (Section II-A4) between Gaussian components of the palette and target distributions.

Method Name	Ref.	Corr.	No Corr.	Code availability for testing	Image	Video	Test $P \simeq T$ (Sec. IV-A)	Test $P \neq T$ (Sec. IV-B)
Ours		yes	yes	<a href="https://www.scss.tcd.ie/~mgogan/colourtransfer.html">https://www.scss.tcd.ie/~mgogan/colourtransfer.html</a>	yes	yes	yes	yes
Bonneel	[6]	no	yes	<a href="https://github.com/gpeyre/2014-JMIV-SlicedTransport">https://github.com/gpeyre/2014-JMIV-SlicedTransport</a>	yes	no	yes	yes
PMLS	[7]	yes	no	Results for this method in this paper have been processed by the authors of [7]	yes	yes	yes	no
Ferradans	[8]	no	yes	<a href="https://github.com/gpeyre/2013-SIIMS-regularized-ot">https://github.com/gpeyre/2013-SIIMS-regularized-ot</a>	yes	no	no	yes
Pitié	[9]	no	yes	<a href="https://github.com/frcs/colour-transfer">https://github.com/frcs/colour-transfer</a>	yes	no	yes	yes

TABLE I

ROAD-MAP FOR EXPERIMENTS. OUR FRAMEWORK IS ABLE TO TAKE ADVANTAGE OF CORRESPONDENCES (CORR) BETWEEN TARGET (T) AND PALETTE (P) IMAGES WHEN AVAILABLE, AND WITHOUT CORRESPONDENCES (NO CORR). WHILE CORRESPONDENCES ARE EASILY AVAILABLE WHEN PALETTE AND TARGET IMAGES CAPTURE THE SAME VISUAL CONTENT ( $P \simeq T$ ), THEY ARE NOT AVAILABLE WHEN USING IMAGES OF DIFFERENT CONTENT ( $P \neq T$ ).

1) *Registration of colour statistical moments*: The pioneering work of Reinhard et al. [5] proposed to use a warping function  $\phi$  with parametric form [5]:

$$\phi(x, \theta = \{G, o\}) = Gx + o \quad (1)$$

with the vector  $o$  representing an offset and the  $3 \times 3$  diagonal matrix  $G$  representing the gains for each colour channel. The estimation of the parameter  $\theta$  is performed by registering the probability density functions of the colour in the palette and target images, denoted  $p_p$  and  $p_t$ , represented as simple multivariate Gaussians ( $p_p \equiv \mathcal{N}(x; \mu_p, \Sigma_p)$  and  $p_t \equiv \mathcal{N}(x; \mu_t, \Sigma_t)$ ) with diagonal covariance matrices  $\Sigma_p$  and  $\Sigma_t$ . Since Normal distributions are fully described by their first two statistical moments, means and covariance matrices, the optimal mapping  $\phi$  is specified by the solution  $\hat{\theta}$  that maps the empirical estimates of  $(\mu_t, \Sigma_t)$  computed using the pixels values  $\{x_t^{(i)}\}_{i=1, \dots, n_t}$  in the target image, to the empirical estimates of  $(\mu_p, \Sigma_p)$  computed using the pixels values  $\{x_p^{(i)}\}_{i=1, \dots, n_p}$  in the palette image.

2) *Optimal transport*: Monge’s formulation [10] sets the deterministic decoupling  $y = \phi(x)$  linking two random variables  $y \sim p_t(y)$  and  $x \sim p_p(x)$  imposing the solution  $\phi$  that verifies [11]:

$$p_p(x) = p_t(\phi(x)) \times |\det \nabla \phi(x)| \quad (2)$$

In practice, finding  $\phi$  such that equation (2) is true is difficult when considering multidimensional space [11]. A solution when  $x \in \mathbb{R}$  and  $y \in \mathbb{R}$  can however be defined with the cumulative distribution of colours in the target and palette images  $P_t$  and  $P_p$ :

$$\phi(x) = P_t^{-1} \circ P_p(x) \quad (3)$$

when  $P_t$  is strictly increasing (i.e.  $p_t(y) > 0, \forall y \in \mathbb{R}$ ).  $P_t$  and  $P_p$  can be approximated with cumulative histograms for instance. Such a process for finding the warping function  $\phi$  is powerful since no strong hypotheses are made about the distributions (as opposed to the Gaussian assumption in Section II-A1). Moreover, no parametric form is imposed on the warping function  $\phi$ .

Solution to Eq. (2) becomes non trivial in multidimensional colour spaces. Of particular interest is the pioneering work of Pitié et al. [12] who proposed an iterative algorithm that first projects the colour pixels  $\{x^{(k)}\}$  on a 1D Euclidean space, and then estimate  $\hat{\phi}$  using Eq. (3) and apply it to move all values  $\{x^{(k)}\}$  along the direction of the 1D space. This

operation is repeated with different directions in 1D space until convergence. The intuitive explanation for this approach comes from the Radon transform [9]: if equation (3) is verified in all 1D projective spaces, then Equation (2) will be verified in the multidimensional space. Bonneel et al. [6] recently proposed to use a similar radon transform inspired strategy for colour transfer in their optimal transport method. Their approach is a generalisation of the method proposed by Pitié et al. which uses 1-D Wasserstein distances to compute the barycentre of a number of input measures. As well as being used for colour transfer between target and palette images, their method can also be used to find the barycentre of three or more weighted image palettes.

Optimal transport is now a widely used framework for solving colour transfer as it allows modelling more various, realistic and complex forms for the distributions  $p_t$  and  $p_p$  than simple multivariate Gaussians, and allows for a parameter free form of the warping function  $\phi$  to be estimated. Histograms are often employed to approximate the colour distributions of images [13], [14], [15] and used in optimal transport methods [16], [8], [15]. Similar to the original Pitié algorithm [12], these discrete methods have a tendency to introduce grainy artifacts in the gradient of the result image. Pitié et al’s subsequent extension [9] proposed a post processing step to correct this artifact and ensure the gradient field of the recoloured target image is as close as possible to the original target image. Similarly, recent methods have proposed adding a step to impose that the resulting spatial gradient of the recoloured image remains similar to the target image [17], [14], [8]. Alternatively other methods have proposed to relax the constraint that enforces the distributions of the recolored target image and palette image to match exactly [16], [15], [8]. Bonneel et al. [6] also propose using a gradient smoothing technique to reduce any quantisation errors that appear in their results [18]. Frigo et al. [19] propose to remove artifacts by first estimating an optimal transport solution and using it to compute a smooth Thin Plate Spline (TPS) transformation to ensure that a smooth parametric warping function is used for recolouring allowing them to apply their method to video content easily.

3) *Using Gaussian Mixture models*: Jeong and Jaynes [20] use colour transfer techniques to harmonise the colour distributions of non overlapping images of the same object for tracking purposes in a multiple camera setting. Colour chrominance (2D) distribution is modelled using Gaussian

Mixture models, and the transfer function is parametric with an affine form estimated by minimising the Kullback-Leibler divergence between Gaussian Components with a robust procedure to tackle outlier pairs. Xiang et al. [21] model the colour distribution of the target image with a Gaussian mixture estimated by an EM algorithm. Each Gaussian component in the mixture defines a local region in the target image, and each segmented local region is recoloured independently using multiple palette-source images, likewise segmented in regions using GMM fitting of their colour distributions. Colour transfer is performed by associating the best Gaussian component from the sources to the Gaussian target region using Reinhard's Gaussian affine transfer function [5]. Segmentation using alternative approaches (i.e. Mean Shift [22], K-means [23]) is also tested to define the colour Gaussian mixtures. This approach relies on homogeneous colour regions, each captured with one multivariate normal in the 3D colour space. Localised colour transfer using Gaussian Mixture models between overlapping colour images have also been proposed for colour corrections, motion deblurring, denoising, gray scale coloring [24].

4) *Using correspondences*: Using one to one correspondence between a Gaussian component capturing the colour content of the target image and palette images (or their regions) have been used for estimating an affine warping function  $\phi$ . Other methods which take correspondences into account when finding the colour transformation include [25], [26], [7]. Oliveira et al. [25] proposed to find the mapping of 1-dimensional truncated GMM representations computed for each colour channel of the target and palette images. Hwang et al. [7] use moving least squares to estimate an affine transformation for each pixel in the target image with the least squares algorithm. To tackle sensitivity to outlier correspondences, only subsets of the correspondences are used as control points and a probabilistic framework is deployed to remove correspondences that are likely to be incorrect. However both of these methods are only applicable when the correspondences between target pixels and palette pixels are available.

## B. Shape registration

In this section, we consider shapes as entities mathematically described as a set of  $n$  contour points in 2D, and as a set of  $n$  vertices on the surfaces of objects in 3D [27]. A shape is hence denoted as a point cloud  $\{x^{(i)}\}_{i=1, \dots, n}$ , where the point description  $x^{(i)}$  corresponds to the 2D or 3D coordinates in the spatial domain. This description can, however, be augmented with additional information such as the local normal direction to the contour or surface [28]. In the past decade or so, several shape registration techniques have been formulated as minimising a divergence between probability density functions capturing the target shape,  $p_t(x)$ , and a model shape,  $p_p(x)$ , by finding the parametric deformation  $\phi$  to apply to the target shape to register it on the model shape (Section II-B3). The probability density functions  $p_t$  and  $p_p$  can be approximated by kernel density estimates using observations  $\{x_t^{(i)}\}_{i=1, \dots, n_t}$  and  $\{x_p^{(i)}\}_{i=1, \dots, n_p}$  describing the two shapes to be registered. Several kernels, such as the Gaussian kernel, are easier to use

for registration (Section II-B2). Many dissimilarity metrics have been defined for pdfs and the Kullback-Leibler divergence, already mentioned to solve colour transfer, is probably the most well known [29]. Section II-B1 proposes instead a more robust alternative to Kullback Leibler divergence for comparing pdfs that corresponds to the Euclidean  $\mathcal{L}_2$  distance between these pdfs. Some correspondences between the target and model shapes, denoted  $\{(x_t^{(k)}, x_p^{(k)})\}_{k=1, \dots, n}$  with  $n \leq n_t$  and  $n \leq n_p$ , may occasionally be available and can also be efficiently used with the  $\mathcal{L}_2$  distance (Section II-B4).

1)  $\mathcal{L}_2$  distance: The Euclidean  $\mathcal{L}_2$  distance between two pdfs is defined as:

$$\mathcal{L}_2 = \|p_t - p_p\|^2 = \int (p_t(x) - p_p(x))^2 dx \quad (4)$$

and it can be conveniently rewritten  $\mathcal{L}_2 = \|p_t\|^2 - 2\langle p_t | p_p \rangle + \|p_p\|^2$ . Of note the term  $\|p\|^2$  is proportional to the quadratic Renyi entropy of  $p$  (for target and palette), while the scalar product term  $\langle p_t | p_p \rangle$  is proportional to the Renyi cross entropy between  $p_t$  and  $p_p$  [29]. The advantage of computing  $\mathcal{L}_2$  over the Kullback Leibler divergence between probability density functions is that it can be computed explicitly with Gaussian mixtures and it has also been shown to be more robust to outliers [27], [30].

2) *GMM representation of shapes*: Gaussian Mixture Models have been a popular representation of shapes for solving shape registration [29]. Recently Jian et al. [31], [27] proposes to register two point cloud shapes  $\{x_t^{(i)}\}_{i=1, \dots, n_t}$  and  $\{x_p^{(i)}\}_{i=1, \dots, n_p}$ , by first fitting a kernel density estimate to each point set using the Gaussian kernel. The target distribution is formulated as [31], [27]:

$$p_t(x|\theta) = \frac{1}{n_t} \sum_{i=1}^{n_t} \mathcal{N}(x; \phi(x_t^{(i)}, \theta), h^2 \mathbf{I}) \quad (5)$$

with notation  $\mathcal{N}(x; \mu, \Sigma)$  indicating a Normal distribution for random vector  $x$ , with mean  $\mu$  and covariance  $\Sigma$ . The function  $\phi(x, \theta) = \phi_\theta(x)$  moves vertex  $x_t^{(i)}$  and this displacement is controlled by a latent vector  $\theta$  to be estimated. The second kernel density estimate is defined using the second point set as:

$$p_p(x) = \frac{1}{n_p} \sum_{i=1}^{n_p} \mathcal{N}(x; x_p^{(i)}, h^2 \mathbf{I}). \quad (6)$$

Isotropic covariance matrices controlled by a bandwidth  $h$  (with  $\mathbf{I}$  a  $3 \times 3$  identity matrix) are used for both distributions. The estimation of the warping function  $\phi$  consists of finding  $\theta$  that minimises the  $\mathcal{L}_2$  distance between  $p_p$  and  $p_t$ :

$$\hat{\theta} = \arg \min_{\theta} \{ \|p_t\|^2 - 2\langle p_t | p_p \rangle \} \quad (7)$$

since  $\|p_p\|^2$  does not depend on  $\theta$  [30]. Terms  $\|p_t\|^2$  and  $\langle p_t | p_p \rangle$  can be computed explicitly using the integral result for Normals:

$$\int \mathcal{N}(x; \mu_1, \Sigma_1) \mathcal{N}(x; \mu_2, \Sigma_2) dx = \mathcal{N}(0; \mu_1 - \mu_2, \Sigma_1 + \Sigma_2)$$

3) *Deformable transfer function  $\phi$* : The transfer function  $\phi : x \in \mathbb{R}^d \rightarrow \phi_\theta(x) \in \mathbb{R}^d$  can be conveniently defined as a rigid, affine or Thin Plate Splines parametric function [29], [27] which can be written as:

$$\phi_\theta(x) = \underbrace{Ax + o}_{\text{Affine}} + \underbrace{\sum_{j=1}^m w_j \psi(\|x - c_j\|)}_{\text{nonlinear}} = Ax + o + W \Psi(x) \quad (8)$$

Discarding the non linear part of  $\phi$  provides an affine warping function which can be further limited to a rigid transformation by choosing  $A$  as a rotation matrix. For the more general TPS form, the latent parameters of interest,  $\theta$ , corresponds to the set of coefficients  $\{w_j \in \mathbb{R}^d\}$ , the  $d \times d$  matrix  $A$  and the  $d$ -dimensional vector offset  $o$ . The non linear part can be rewritten in matrix form with a  $d \times m$  matrix  $W$  gathering coefficients  $\{w_j \in \mathbb{R}^d\}$ , and an  $m$  dimensional vector  $\Psi(x)$  collating all values  $\{\psi(\|x - c_j\|) = -\|x - c_j\|\}$ . The set of control points  $\{c_j\}_{j=1, \dots, m}$  are a subset of the observations  $\{x^{(i)}\}$  [27]. Other deformable models (linear in  $x$  and  $\theta$ ) have been used with  $\mathcal{L}_2$  to register shapes [32], [33]. These models rely on Principal Component Analysis to learn deformations of a family of shapes. Regularisation terms can also be added to  $\mathcal{L}_2$  to constraint the estimation of  $\theta$  [27], [32].

4) *Using correspondences*: Finding correspondences between shapes can be done using local descriptors such as shape context for point clouds [34], or using SIFT features [35] when considering images for instance. Ma et al. [36] have proposed to use only the correspondences for performing shape registration with  $\mathcal{L}_2$  to improve both robustness and computational efficiency.

### C. Remarks

Shapes described as point clouds in the spatial domain (2D or 3D) have the same mathematical representation as colour pixels values of an image represented as points in a 3D colour space. Therefore the methods presented in Section II-B for registering point cloud shapes can be used to register point clouds of colour triplets of a target and palette images. This is the core idea of this paper with more details for its implementation given in paragraph III.

Pitié et al. have also shown experimentally that their original optimal transport algorithm for colour transfer iteratively decreases the Kullback Leibler divergence between the probability density functions  $p_t$  and  $p_p$  [9]. As an alternative, we instead propose to explicitly formulate the problem of colour transfer as minimising a divergence ( $\mathcal{L}_2$ ) between pdfs.

Pitié et al's non parametric formulation of the solution  $\hat{\phi}$  gives, for each pixel  $x_t^{(i)}$ , a corresponding value  $\hat{\phi}(x_t^{(i)})$  but does not provide the possibility of applying this transformation to a previously unseen value  $x$  [9]. Moreover the warping function  $\hat{\phi}$  cannot be directly manipulated for mixing with other estimated warping functions. Alternatively, a parametric affine warping function  $\phi_\theta$  can be computed directly with the optimal transport framework [37]. However this computation assumes that target and palette pdfs are Normals which is a gross approximation of colour distributions in images in

general. Moreover affine warping functions are limited for registering colour statistics, and as an improvement, Frigo et al. [19] has proposed instead to fit a smooth Thin Plate Spline (TPS) transformation to the non parametric optimal transport solution to propose a more complex non rigid warping function  $\phi_\theta$  suitable for colour transfer.

## III. ROBUST COLOUR TRANSFER

### A. GMM representation of colour content

We define two Gaussian mixture models  $p_t(x)$  and  $p_p(x)$  capturing the colour content of the target and palette image respectively as follows (omitting subscript  $(t, p)$ ):

$$p(x) = \sum_{k=1}^K \mathcal{N}(x; \mu^{(k)}, \Sigma^{(k)}) \pi^{(k)} \quad (9)$$

with  $K \in \{K_t, K_p\}$  the number of Gaussians in the mixture for the target and palette images,  $\mu^{(k)} \in \{\mu_t^{(k)}, \mu_p^{(k)}\}$  the respective means and  $\Sigma^{(k)} \in \{\Sigma_t^{(k)}, \Sigma_p^{(k)}\}$  covariances of the Gaussian  $k$ . The coefficients  $\pi^{(k)} \in \{\pi_t^{(k)}, \pi_p^{(k)}\}$  are positive weights, all summing to one, capturing the relative importance of each Gaussian component in the mixture. The target distribution  $p_t(x)$  is changed to a parametric family of distributions  $p_t(x|\theta)$  by changing the means  $\{\mu_t^{(k)}\}$  to  $\{\phi(\mu_t^{(k)}, \theta)\}$ . The Renyi cross entropy term in  $\mathcal{L}_2$  is then proportional to:

$$\langle p_t | p_p \rangle = \sum_{k=1}^{K_t} \sum_{l=1}^{K_p} \mathcal{N}(0; \phi(\mu_t^{(k)}, \theta) - \mu_p^{(l)}, \Sigma_t^{(k)} + \Sigma_p^{(l)}) \pi_t^{(k)} \pi_p^{(l)} \quad (10)$$

while the quadratic entropy of  $p_t$  is proportional to:

$$\|p_t\|^2 = \sum_{k=1}^{K_t} \sum_{l=1}^{K_t} \mathcal{N}(0; \phi(\mu_t^{(k)}, \theta) - \phi(\mu_t^{(l)}, \theta), \Sigma_t^{(k)} + \Sigma_t^{(l)}) \pi_t^{(k)} \pi_t^{(l)} \quad (11)$$

Jian et al. use  $\mathcal{L}_2$  to register shapes encoded as Gaussian Kernel Density Estimates [27]. Using this idea for our colour transfer application would mean that the number  $K$  of Gaussians in the mixture (Eq. 9) is the number of pixels in the image (target or palette), and the cluster centres  $\mu^{(k)} = x^{(k)}$  are the colour pixels  $x^{(k)}$  in the image. In this case  $K$  is extremely large and our cost function becomes too computationally intensive to be practical. As an alternative two algorithms for clustering, K-means and Mean Shift, are proposed to compute the means (Sections III-B and III-C). When correspondences are available between palette and target images, a third method for setting the means is proposed in Section III-D.

1) *Covariances*: Both target and palette GMMs uses isotropic identical covariance matrices controlled by a bandwidth  $h$ :

$$\Sigma = h^2 \mathbf{I} \quad (12)$$

with the identity matrix  $\mathbf{I}$ . In this case the scalar product between two Normal distributions is:

$$\langle \mathcal{N}(\mu_1, h^2 \mathbf{I}) | \mathcal{N}(\mu_2, h^2 \mathbf{I}) \rangle = \mathcal{N}(0; \mu_1 - \mu_2, 2h^2 \mathbf{I}) \quad (13)$$

and when  $h$  is very large the Taylor series expansion of  $e^{-x}$  can be used to compute the approximation:

$$e^{-\frac{(\mu_1 - \mu_2)^2}{4h^2}} \simeq 1 - \frac{1}{4h^2} (\mu_1 - \mu_2)^2 \quad (14)$$

Finding  $\theta$  corresponds in this case to minimising the quadratic convex function:

$$\begin{aligned} \|p_t\|^2 - 2\langle p_t | p_p \rangle &\simeq - \sum_{k=1}^{K_t} \sum_{l=1}^{K_t} \left( \frac{\phi(\mu_t^{(k)}, \theta) - \phi(\mu_t^{(l)}, \theta)}{2h} \right)^2 \pi_t^{(k)} \pi_t^{(l)} \\ &+ 2 \sum_{k=1}^{K_t} \sum_{l=1}^{K_p} \left( \frac{\phi(\mu_t^{(k)}, \theta) - \mu_p^{(l)}}{2h} \right)^2 \pi_t^{(k)} \pi_p^{(l)} - 1 \quad (15) \end{aligned}$$

This cost function is a trade off between moving  $\mu_t$ s as close as possible to  $\mu_p$ s (Renyi cross entropy term), while avoiding collapsing all  $\mu_t$ s to a sole mean vector (quadratic Renyi entropy term). In other words, the target pdf  $p_t$  is prevented from collapsing into a unique Gaussian distribution and for keeping the  $p_t$  as spread as possible over the colour space. The bandwidth  $h$  is also used as a temperature in our algorithm (starting with a large value of  $h$ ) when estimating  $\theta$  in a simulated annealing framework to avoid local solutions.

2) *Weights*: The natural choice for setting the weights  $\pi^{(k)}$  is to choose the proportion of pixels in the image associated with the cluster  $k$ . However since target and palette images do not have exactly the same visual content in general, as in [19] we found that matching the colour content of the images was preferable to matching the true colour distribution of the images. Therefore we choose equal weights for each cluster and set  $\pi^{(k)} = \frac{1}{K}$ .

### B. K-means Algorithm

The K-means clustering algorithm can be used to define  $\{\mu^{(k)}\}$  for both target and palette images [1], [2]. The computational complexity is then controlled when choosing the number  $K$  of clusters in the pixels values sets  $\{x_t^{(i)}\}_{i=1, \dots, n_t}$  and  $\{x_p^{(i)}\}_{i=1, \dots, n_p}$ . The K-means algorithm is equivalent to using an EM algorithm enforcing identical isotropic covariance matrices [38].

### C. Mean Shift Segmentation

A possible alternative to K-means is the Mean Shift clustering algorithm which has been previously proposed in other colour transfer techniques for image segmentation [25], [21] and takes into account spatial information when computing the cluster centres  $\{\mu^{(k)}\}$  [22]<sup>1</sup>. The Mean Shift algorithm can also be thought of as an EM algorithm [39].

### D. Correspondences

Pixel pairs between target and palette images, denoted  $\{(x_t^{(k)}, x_p^{(k)})\}_{k=1, \dots, n}$ , can be computed when considering target and palette images capturing the same scene. Colour transfer techniques are indeed often used in this context to harmonise colours across a video sequence and/or across multiple view images such as in the bullet time visual effect. In this case, the means of the Gaussian mixtures are set such that

$\{(\mu_t^{(k)}, \mu_p^{(k)}) = (x_t^{(k)}, x_p^{(k)})\}_{k=1, \dots, n}$  imposing  $K_t = K_p = n$  when defining the distributions  $p_t$  and  $p_p$ . Moreover, the scalar product  $\langle p_t | p_p \rangle$  in our cost function is then simplified as follows:

$$\langle p_t | p_p \rangle = \sum_{k=1}^n \mathcal{N}(0; \phi(\mu_t^{(k)}, \theta) - \mu_p^{(k)}, \Sigma_t^{(k)} + \Sigma_p^{(k)}) \pi_t^{(k)} \pi_p^{(k)} \quad (16)$$

The computational complexity of this term is then  $n = K_t = K_p$  when using  $n$  correspondences, and  $K_t \times K_p$  without correspondences. Performance of our approach with correspondences is assessed in Section IV using palette and target images with similar content. Pixel correspondences are not used when considering palette and target images with different content but K-means or Mean Shift clustering are used instead.

### E. Warping function $\phi$

RBF name	RBF equation
TPS	$\psi(r) = -(r)$
Gaussian	$\psi(r) = e^{-(\epsilon r)^2}$
Inverse Multiquadric	$\psi(r) = \frac{1}{\sqrt{1+(\epsilon r)^2}}$
Inverse Quadric	$\psi(r) = \frac{1}{1+(\epsilon r)^2}$

TABLE II  
THE EQUATIONS FOR THE DIFFERENT RADIAL BASIS FUNCTIONS  $\psi$   
TESTED IN THIS PAPER.

In this paper, several radial basis functions  $\psi$  are tested including TPS to define the warping function  $\phi$  (cf. Eq. 8). Possible choices for  $\psi$  are listed in Table II. The colour spaces considered for testing our framework are the RGB and Lab spaces. In both cases, the  $m$  control points  $\{c_j\}_{j=1, \dots, m}$  are chosen on a regular grid spanning the 3D colour space such that the 3D grid has  $m = 5 \times 5 \times 5 = 125$  control points in the colour space. As a consequence the dimension of the latent space to explore for the estimation of  $\theta$  is:

$$\dim(\theta) = 125 \times 3 + 9 + 3 = 387$$

with  $\dim(c_j) = 3$ ,  $\forall j$ ,  $\dim(A) = 3 \times 3 = 9$  and  $\dim(o) = 3$  (cf. Eq. 8).

### F. Estimation of $\theta$

To enforce that a smooth solution  $\phi$  is estimated, the Euclidean distance  $\mathcal{L}_2(\theta)$  is minimised with a roughness penalty on the transfer function  $\phi$  [29] and the estimation is performed as:

$$\hat{\theta} = \arg \min_{\theta} \left\{ \mathcal{C}(\theta) = \|p_t\|^2 - 2\langle p_t | p_p \rangle + \lambda \int \|D^2 \phi(x, \theta)\|^2 dx \right\} \quad (17)$$

with  $\|D^2 \phi(x, \theta)\|^2 = \sum_{i, j \in \{1, \dots, d\}} \left( \frac{\partial^2 \phi}{\partial x_i \partial x_j} \right)^2$  with  $d = 3$  for the colour spaces.

<sup>1</sup>Code for [22] at <http://coewww.rutgers.edu/riul/research/code.html>

### G. Implementation Details

Our strategies to estimate  $\theta$  are summarised in Algorithm 1.

---

**Algorithm 1** Our strategies for estimating the parameter  $\theta$  for the warping function  $\phi_\theta(x)$ .

---

**Require:**  $\hat{\theta}$  initialised so that  $\phi_{\hat{\theta}}(x) = x$  (identity function)

**Require:**  $hmin$ ,  $hmax$ ,  $\lambda$  and choose  $\psi$  (with  $\epsilon$ )

**Require:** Initialisation of  $\{\mu_t^{(i)}\}$ ,  $\{\mu_p^{(i)}\}$  or  $\{(\mu_t^{(i)}, \mu_p^{(i)})\}$  (correspondences)

**if** Using K-means (no correspondences) **then**

choose  $K_t$  and  $K_p$

Cost function  $\mathcal{C}(\theta)$  (Eq. 17) defined with term  $\langle p_t | p_p \rangle$  (Eq. 10)

**else if** Using Mean Shift (no correspondences) **then**

$K_t$  and  $K_p$  are estimated by Mean Shift

Cost function  $\mathcal{C}(\theta)$  (Eq. 17) defined with term  $\langle p_t | p_p \rangle$  (Eq. 10)

**else if** Using  $n$  correspondences **then**

$K_t = K_p = n$

Cost function  $\mathcal{C}(\theta)$  (Eq. 17) defined with term  $\langle p_t | p_p \rangle$  (Eq. 16)

**end if**

Start  $h = hmax$  (controls covariance matrix Eq. 12)

**repeat**

$\hat{\theta} \leftarrow \arg \min_{\theta} \mathcal{C}(\theta)$

$h \leftarrow .5 \times h$  (annealing)

**until** Convergence  $h < hmin$  **return**  $\hat{\theta}$

---

Two values,  $\lambda$  and  $\epsilon$  (in the case of the Gaussian, Inverse Quadric and Inverse Multiquadric basis functions as defined in Tab. II) need to be chosen in our framework. Table III gives the values that were used in our experiments to get the best results overall. For clarity we extend that notation in Table

RBF $\psi$ and colour space	Correspondences		No Correspondences	
	$\lambda$	$\epsilon$	$\lambda$	$\epsilon$
TPS <sub>rgb</sub>	$3e^{-3}$	<b>X</b>	$3e^{-6}$	<b>X</b>
TPS <sub>lab</sub>	$3e^{-3}$	<b>X</b>	$3e^{-4}$	<b>X</b>
G <sub>rgb</sub>	$3e^{-5}$	$6e^{-3}$	$3e^{-8}$	$6e^{-3}$
G <sub>lab</sub>	$6e^{-3}$	3	$3e^{-4}$	3
InMQ <sub>rgb</sub>	$3e^{-5}$	$6e^{-3}$	$3e^{-8}$	$6e^{-3}$
InMQ <sub>lab</sub>	$6e^{-3}$	10	$3e^{-4}$	3
InQ <sub>rgb</sub>	$3e^{-6}$	$6e^{-3}$	$3e^{-8}$	$6e^{-3}$
InQ <sub>lab</sub>	$6e^{-3}$	30	$3e^{-4}$	3

TABLE III

SELECTED PARAMETERS  $\lambda$  AND  $\epsilon$  IN OUR ALGORITHMS TESTED IN OUR EXPERIMENTS IN SECTION IV. IN ADDITION, THE NUMBER OF CLUSTERS FOR K-MEANS IS SET TO  $K_t = K_p = 50$ , WHILE THE NUMBER OF CORRESPONDENCES  $n = 50000$  ARE CHOSEN RANDOMLY ACROSS THE OVERLAPPING REGION OF THE TARGET AND PALETTE IMAGES AFTER REGISTRATION. WHEN MEAN SHIFT CLUSTERING IS USED, THE NUMBER OF CLUSTERS ( $K_t$  AND  $K_p$ ) ARE ESTIMATED ALONG WITH THE CLUSTER CENTRES.

III so that TPS<sub>rgb</sub><sup>KM</sup> indicates the basis function  $\psi$  is TPS, the colour space is RGB, and the clustering techniques for finding the means of the GMMs is K-means (similarly denote TPS<sub>rgb</sub><sup>MS</sup> for Mean Shift and TPS<sub>rgb</sub><sup>Corr</sup> when using Correspondences).

### H. Parallel Recolouring step

One of the main advantages of this method is the fact that our transformation is controlled by a parameter  $\theta$  and any pixel  $x$  can be recoloured by computing the new colour value  $\phi_\theta(x)$ . This computation can be done in parallel by distributing the pixels to be recoloured to the multiple processors that are available. Moreover, with one target image and  $N$  palette images of choice, the transformations  $\{\hat{\theta}_1, \dots, \hat{\theta}_N\}$  can also be estimated in parallel, and any interpolated new value  $\theta$  can be used for recolouring:

$$\theta_{new} = \sum_{j=1}^N \gamma_j \hat{\theta}_j, \quad \text{with } \sum_{j=1}^N \gamma_j = 1, \text{ and } \gamma_j \geq 0 \forall j \quad (18)$$

Interpolating in the  $\theta$  space to create a new warping function is made easy thanks to the fact that we chose control points on a regular grid (cf. Section III-E) and not as sub samples of palette images (cf. Section II-B3). Of particular interest are the creation of smooth temporal transitions between the identity warping function and a colouring warping function for instance. In Section V-A we show more on how to create visual effects using interpolation masks. Having a quick recolouring step is essential to give the user instant feedback about the new effects being applied to the image or video. Our transformation can be applied to each pixel independently and it is therefore highly parallelisable. A CPU or GPU parallel implementation would ensure that the target image is recoloured almost instantly. For our implementation we parallelised the recolouring step on the CPU using OpenMP, and performance is assessed in Section IV-D.

## IV. EXPERIMENTAL RESULTS

To quantitatively assess recolouring results, three metrics, peak signal to noise ratio (PSNR), structural similarity index (SSIM) and colour image difference (CID), are often used when considering palette and target images of the same content for which correspondences are easily available [25], [7], [40]. Alternatively user studies have also been used to assess the perceptual visual quality of the recolouring [41].

We evaluate our proposed algorithms and show that they are comparable to current state of the art colour transfer algorithms in terms of the perceptual quality of the results (paragraphs IV-A, IV-B and IV-C), and superior in terms of computational speed (paragraph IV-D). Moreover our parametric formulation for colour transfer allows easy and flexible manipulations by artists for creating new visual effects (paragraph V-A). When carrying out our colour transfer algorithm in Lab space<sup>2</sup>, both the clustering and registration is performed in Lab space, with the results converted back to RGB before the metrics are computed.

Table I summarises the methods (including ours) used for comparison in this paper.

<sup>2</sup>Matlab functions rgb2lab and lab2rgb with reference white point ‘d65’ used when converting RGB and Lab, and vice versa.

### A. Images with similar content $P \simeq T$

One important application of colour transfer is in harmonising the colour palette of several images or videos capturing the same scene. To evaluate our algorithm applied to images with similar content, we use the 15 images in the dataset provided by Hwang et al. [7]<sup>3</sup> which includes images with many different types of colour changes including different illuminations, different camera settings and different colour touch up styles. This dataset provides palette images which have been aligned to match the target image (c.f. Figure 2). To define correspondences, pixels at the same location in the target and aligned palette images are selected together to form a pair [7].

1) *Choice of radial basis function  $\psi$* : Table IV provides quantitative metrics to evaluate our algorithms with correspondences using the PSNR, SSIM and CID metrics<sup>4</sup>. In general

	PSNR		SSIM		CID	
	$\mu$	$SE$	$\mu$	$SE$	$\mu$	$SE$
$TPS_{rgb}^{Corr}$	30.30	1.5	0.944	0.02	0.172	0.02
$TPS_{lab}^{Corr}$	30.56	1.4	0.942	0.02	0.182	0.03
$G_{rgb}^{Corr}$	30.03	1.5	0.944	0.02	0.176	0.02
$G_{lab}^{Corr}$	30.56	1.4	0.942	0.02	0.184	0.03
$InMQ_{rgb}^{Corr}$	30.37	1.5	0.944	0.02	0.173	0.02
$InMQ_{lab}^{Corr}$	30.49	1.4	0.942	0.02	0.183	0.03
$InQ_{rgb}^{Corr}$	30.37	1.5	0.944	0.02	0.169	0.02
$InQ_{lab}^{Corr}$	30.22	1.4	0.940	0.02	0.188	0.02

TABLE IV

ASSESSMENT OF OUR ALGORITHMS USING CORRESPONDENCES WITH SEVERAL BASIS FUNCTIONS  $\psi$  IN TWO COLOUR SPACES. THE MEAN PSNR, SSIM AND CID VALUES  $\mu$ , AND STANDARD ERROR  $SE$ , FOR EACH METHOD COMPUTED ON THE 15 IMAGES IN THE DATASET. HIGHEST PSNR AND SSIM VALUES, AND LOWEST CID VALUES, INDICATE THE BEST RESULTS (BEST IN RED, SECOND BEST IN GREEN, THIRD BEST IN BLUE).

the methods applied in the Lab colour space provide slightly better results in terms of PSNR, and slightly worse results in terms of SSIM and CID. A t-test comparing the mean values of each method confirms though that the difference between them is statistically insignificant (with 99% confidence). TPS has the advantage of being faster to compute (paragraph IV-D) and since it achieves perceptually similar performance, it is mainly used for comparison in the rest of the paper.

2) *With or without correspondences*: Table V compares  $TPS_{rgb}$  with correspondences ( $TPS_{rgb}^{Corr}$ ) to stress that using correspondences allows the algorithm to outperform our alternative algorithms that do not use them ( $TPS_{rgb}^{KM}$  and  $TPS_{rgb}^{MS}$ ). Note however that there is no statistical difference in terms of PSNR, SSIM and CID between the results of  $TPS_{rgb}^{KM}$  using K-means and  $TPS_{rgb}^{MS}$  using Mean Shift on this test where palette and target images capture the same scene. Section IV-B will show how  $TPS_{rgb}^{KM}$  gives perceptually more pleasing results than  $TPS_{rgb}^{MS}$  for images of different content.

3) *Robustness of  $\mathcal{L}_2$  to outlier correspondences*: To evaluate the robustness of the  $\mathcal{L}_2$  metric, we applied  $TPS_{rgb}^{Corr}$  to images that had many false correspondences. Taking the registered palette and target images, we applied a horizontal

	$TPS_{rgb}^{Corr}$	$TPS_{rgb}^{KM}$	$TPS_{rgb}^{MS}$
PSNR	30.30 (1.5)	24.20 (0.8)	24.47 (0.8)
SSIM	0.944 (0.02)	0.908 (0.02)	0.896 (0.02)
CID	0.172 (0.02)	0.325 (0.02)	0.337 (0.03)

TABLE V

THE MEAN PSNR, SSIM AND CID VALUES FOR THE SET OF IMAGES WITH SIMILAR CONTENT, WITH THE STANDARD ERROR SHOWN IN BRACKETS. USING CORRESPONDENCES LEADS TO BETTER RESULTS.

shift of  $s$  pixels to the target image. Then taking pixels at the same location in the palette and new target image as correspondences we computed the colour transfer result. Figure 1 shows that even when a large number of false correspondences are present, the colours in the result image are very similar to those in the palette image. Areas which have changed colour are long thin structures which no longer have many correct colour correspondences (the blue bars on the tower become green in Figure 1). The structure of the target image has also been well maintained overall.

4) *Comparison to current leading techniques*: Table VI provides a quantitative evaluation of our proposed method (TPS in RGB and Lab spaces) in comparison to leading state of the art colour transfer methods [6], [9], [7]<sup>5</sup> (c.f. notations explained in Table I). In terms of PSNR, SSIM and CID, PMLS performs slightly better in most cases, closely followed by our  $TPS_{rgb}^{Corr}$  and  $TPS_{lab}^{Corr}$  methods but T-tests confirm that there is no significant quantitative difference between PMLS and each of our proposed techniques  $TPS_{rgb}^{Corr}$  and  $TPS_{lab}^{Corr}$  (with a 99% confidence level).

PMLS however introduces some visual artifacts when the content in the target and palette images is not registered exactly. These artifacts can be seen around the car in row 3, column 5 of Figure 2. PMLS is not robust to registration errors, while our algorithm indeed is thanks to the robust  $\mathcal{L}_2$  distance. Our approach allows us to maintain the structure of the original image and to create a smooth colour transfer result (cf. Row 3, column 6 in Fig 2). So to summarise while PMLS and our algorithms provide equivalent quantitative performances as measured by PSNR, SSIM and CID, our techniques in fact provide better qualitative visual results.

### B. Images with different content $P \neq T$

First we compare two methods for estimating the Gaussian means  $\{\mu^{(k)}\}$  - K-means and Mean Shift. In Figure 4 we present the target and palette images recoloured using the  $K$  cluster centres found using these techniques. The cluster centres generated using K-means are evenly spaced throughout the colour distribution of the images and the recoloured images look very similar to the original target and palette. On the other hand, the Mean Shift algorithm takes pixel colour and position into account and the cluster centres therefore depend on the structure of the image. We found that setting the Gaussian mixture means to be the K-means cluster centres gave better results than the Mean Shift clusters as seen in Figure 4. Therefore we present results obtained using the K-means clustering technique in the rest of this section.

<sup>3</sup><https://sites.google.com/site/unimono/pmls>

<sup>4</sup>See supplementary material for image results.

<sup>5</sup>Results using PMLS were provided by the authors of [7].

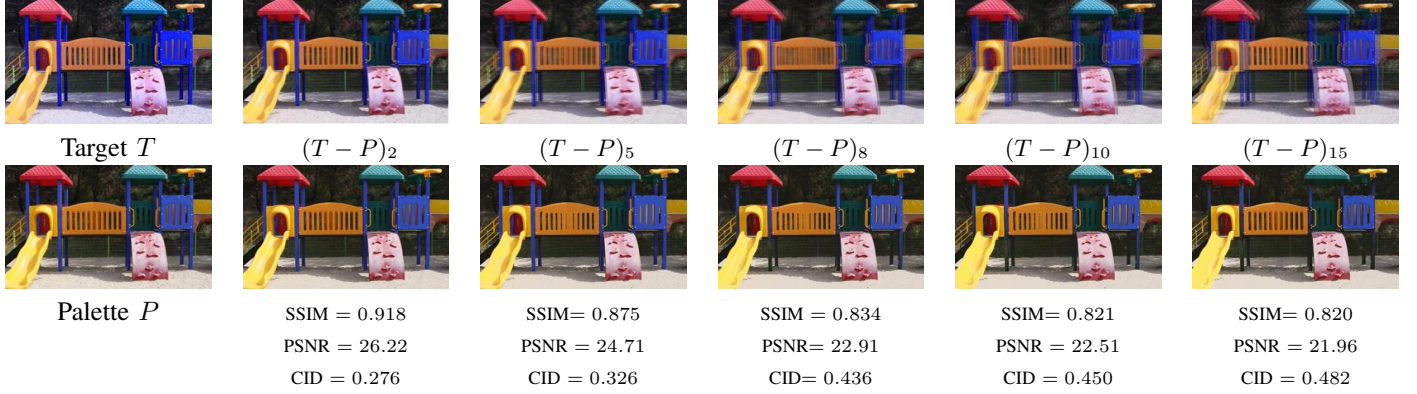


Fig. 1. Robustness of  $\mathcal{L}_2$  with outlier correspondences. The first column gives the target (top) and palette image (bottom). The remaining columns show the colour transfer results of  $\text{TPS}_{rgb}^{Corr}$  when the target image is shifted horizontally by  $s$  pixels, creating incorrect colour correspondences. The top row shows the shifted target superimposed on the palette image  $((T - P)_s)$  and the bottom row shows our colour transfer result with corresponding SSIM, PSNR and CID results.

	PSNR					SSIM					CID				
	Pitié	Bonneel	PMLS	$\text{TPS}_{rgb}^{Corr}$	$\text{TPS}_{lab}^{Corr}$	Pitié	Bonneel	PMLS	$\text{TPS}_{rgb}^{Corr}$	$\text{TPS}_{lab}^{Corr}$	Pitié	Bonneel	PMLS	$\text{TPS}_{rgb}^{Corr}$	$\text{TPS}_{lab}^{Corr}$
building	20.50	12.32	<b>22.63</b>	20.50	22.51	0.807	0.675	<b>0.865</b>	<b>0.862</b>	0.864	0.377	0.383	<b>0.228</b>	0.249	<b>0.271</b>
flower1	24.02	18.42	<b>26.98</b>	26.86	<b>26.85</b>	0.908	<b>0.822</b>	<b>0.967</b>	0.966	0.961	0.395	0.488	<b>0.163</b>	0.174	<b>0.179</b>
gangnam1	24.61	23.86	<b>35.74</b>	<b>35.37</b>	35.70	0.899	0.908	<b>0.992</b>	0.990	<b>0.985</b>	0.237	0.233	<b>0.040</b>	0.048	<b>0.050</b>
gangnam2	26.59	26.82	<b>36.58</b>	35.55	<b>35.51</b>	0.918	0.928	<b>0.993</b>	0.986	<b>0.984</b>	0.250	0.247	<b>0.039</b>	0.089	<b>0.093</b>
gangnam3	22.23	19.69	<b>35.02</b>	33.29	<b>33.10</b>	0.877	0.816	<b>0.991</b>	0.980	<b>0.971</b>	0.442	0.493	<b>0.108</b>	0.193	<b>0.214</b>
illum	19.89	14.34	<b>20.17</b>	<b>19.08</b>	19.84	0.632	0.527	0.649	<b>0.648</b>	<b>0.650</b>	<b>0.390</b>	0.411	0.390	0.397	<b>0.397</b>
mart	22.71	22.15	24.74	<b>24.45</b>	<b>24.92</b>	0.906	0.901	<b>0.957</b>	0.956	<b>0.955</b>	0.513	0.520	<b>0.219</b>	0.225	<b>0.258</b>
playground	27.38	25.96	27.84	<b>27.65</b>	<b>27.91</b>	0.916	0.900	<b>0.940</b>	0.939	<b>0.938</b>	0.378	0.480	<b>0.238</b>	0.254	<b>0.269</b>
sculpture	29.85	22.57	<b>32.06</b>	<b>32.07</b>	<b>32.10</b>	0.942	0.873	<b>0.971</b>	<b>0.972</b>	0.971	0.227	0.390	<b>0.137</b>	0.143	<b>0.161</b>
tonal1	28.55	17.87	<b>37.22</b>	<b>37.33</b>	<b>37.19</b>	0.940	0.852	<b>0.988</b>	0.987	<b>0.987</b>	0.349	0.357	<b>0.101</b>	0.110	<b>0.116</b>
tonal2	27.88	23.00	<b>31.51</b>	31.36	<b>31.33</b>	0.968	0.948	<b>0.987</b>	0.986	<b>0.985</b>	0.294	0.292	<b>0.128</b>	0.145	<b>0.152</b>
tonal3	29.37	16.90	36.25	<b>36.65</b>	<b>36.23</b>	0.961	0.865	0.992	<b>0.992</b>	<b>0.991</b>	0.306	0.418	<b>0.079</b>	0.081	<b>0.083</b>
tonal4	28.57	14.80	<b>34.52</b>	<b>34.34</b>	34.44	0.943	0.812	0.983	<b>0.983</b>	<b>0.983</b>	0.262	0.302	0.108	<b>0.107</b>	<b>0.110</b>
tonal5	30.20	21.08	<b>35.26</b>	<b>34.30</b>	<b>34.96</b>	0.965	0.911	<b>0.986</b>	0.985	<b>0.984</b>	0.185	0.248	<b>0.091</b>	0.092	<b>0.094</b>
$\mu$	25.85	20.07	<b>30.82</b>	<b>30.30</b>	30.56	0.899	0.838	<b>0.946</b>	0.944	<b>0.942</b>	0.330	0.377	<b>0.154</b>	0.172	<b>0.181</b>
$SE$	0.9	1.1	1.5	1.5	1.4	0.02	0.03	0.02	0.02	0.02	0.023	0.024	0.024	0.024	0.025

TABLE VI

COMPARISON OF OUR ALGORITHM  $\text{TPS}_{rgb}^{Corr}$  AND  $\text{TPS}_{lab}^{Corr}$  AGAINST STATE OF THE ART TECHNIQUES. SSIM, PSNR AND CID RESULTS FOR COLOUR TRANSFER TECHNIQUES ON IMAGES WITH SIMILAR CONTENT: HIGHEST PSNR AND SSIM VALUES, AND LOWEST CID VALUES, INDICATE THE BEST RESULTS (BEST IN RED, SECOND BEST IN GREEN, THIRD BEST IN BLUE). THE OVERALL MEAN SCORE  $\mu$  AND ITS STANDARD ERROR  $SE$  FOR EACH METHOD ARE ALSO GIVEN.

We compare our algorithm with other colour transfer techniques [6], [8], [9] applied to images of different content and without correspondences. In the case of Ferradans et al's results, all images were generated using the parameters  $\lambda_X = \lambda_Y = 10^{-3}$  and  $\kappa = (0.1, 1, 0.1, 1)$  [8]. Figure 5 shows that Bonneel and Ferradans methods create blocky artifacts in the result image gradient in some cases (Row 2,4,5). On the other hand, the added constraint in Pitié algorithm which enforces a smooth image gradient ensures that these errors do not appear in their results, creating images that are more visually pleasing. Similarly, the results of our algorithm produce results that match the colours in the palette image well, while still maintaining a smooth image gradient.

Other basis functions, which are more non-linear (see Table IX), have a tendency to fall into local minima when estimating  $\theta$  in our framework when no correspondences are available. Therefore choosing the best parameters (cf. Table III) that create good results for every image is quite difficult. However, when the estimate was the global minimum, the results were

very similar to TPS for both the Lab and RGB colour spaces<sup>6</sup>.

### C. Qualitative assessment

Colour transfer methods have also been evaluated using two subjective user studies, each with 20 participants evaluating 53 sets of images. In each experiment the users were asked to choose the colour transfer result that they thought was the most successful. Out of these 53 sets of images, 38 of them had a palette and target image with different content (no correspondences available), and 15 of them contained a palette and target image with the same content (correspondences available and used). These 15 images were taken from the dataset provided by Hwang et al. (cf. paragraph IV-A). For both user studies, each user evaluated the results individually and the display properties and indoor conditions were kept constant. The order in which the image sets appeared was randomised for each user and a short trial run took place before each user study to ensure the users adapted to the task at hand.

<sup>6</sup>See supplementary material for image results.

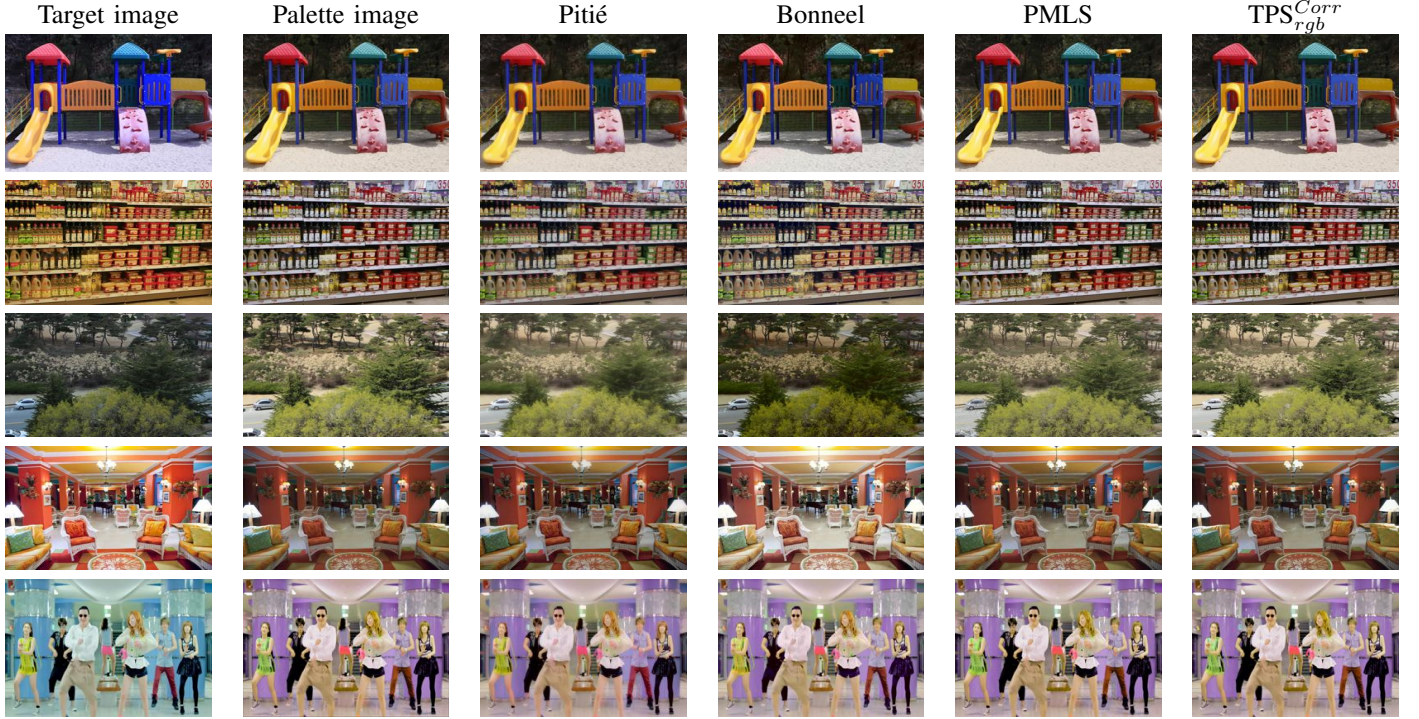


Fig. 2. Results on images with similar content on the ‘playground’, ‘mart’, ‘illum’, ‘tonal4’ and ‘gangnam2’ images. On close inspection grainy artifacts can be seen appearing in some PMLS results. For example, around the car in Row 3 Column 5 or in the top right corner of Row 2 Column 5. In comparison, the results generated by  $TPS_{rgb}^{Corr}$  remain smooth (Column 6). For zoom see Fig. 3.

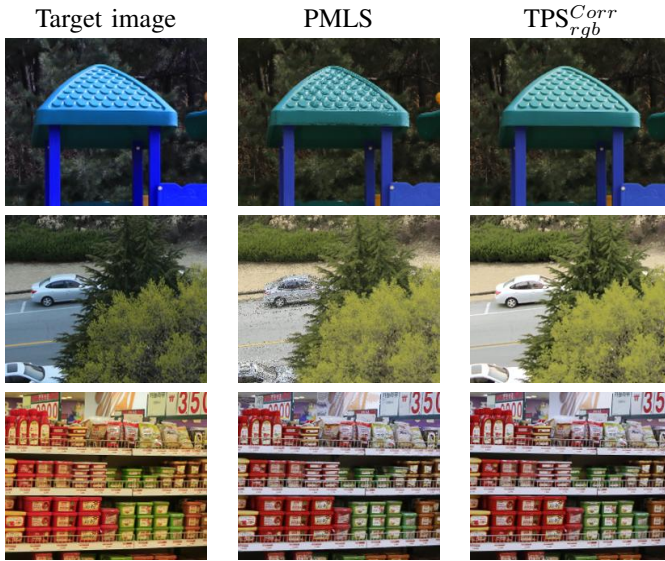


Fig. 3. A close up look at some of the errors generated using PMLS [7] algorithm in comparison to our smooth result with  $TPS_{rgb}^{Corr}$ .

1) *User Study I*: In our first experiment, each participant was presented with six images at a time - a target image, a palette image, and four result images generated using different colour transfer techniques. They then had 20 seconds to view the images (presented simultaneously side by side) and decide which result image was the best. For target and palette images with similar content the four methods compared were  $TPS_{rgb}$ , PMLS, Pitié and Bonneel. The total number of times each

method was chosen can be seen in Table VII. Converting these votes to proportions, we computed confidence intervals on each proportion and compared methods by determining if their confidence intervals overlap. We found that  $TPS_{rgb}$  was the best method in terms of votes however the overlapping confidence intervals indicate that  $TPS_{rgb}$  and PMLS are not statistically significantly different. Hence these two methods can be thought of as performing equally well and both being superior to Pitié and Bonneel methods. Similarly for images with different content we compared  $TPS_{rgb}$ , Ferradans, Pitié and Bonneel. The total number of times each method was chosen can be seen in Table VII. Again, by comparing the confidence intervals on the proportions we determined that  $TPS_{rgb}$  performs better than both Ferradans and Bonneel, however there is no statistically significant difference between  $TPS_{rgb}$  and Pitié.

2) *User Study II*: For our second experiment we used a 2 alternate forced choice (2AFC) comparison. Each participant was presented with two images at a time - a target image, a palette image, and two different result images. They then had 15 seconds to view the images and pick the best result. For target and palette images with similar content we compared two methods -  $TPS_{rgb}$  and PMLS, and the votes are given in Table VIII. Again we converted these votes to proportions and computed the confidence interval on each, and determined that there was no significant difference between the two. We also computed the Thurstone Case V analysis on the votes, which is commonly used to analyse 2AFC results [42]. We computed the preference score and confidence intervals for each method (Table VIII) and found that there is a significant difference

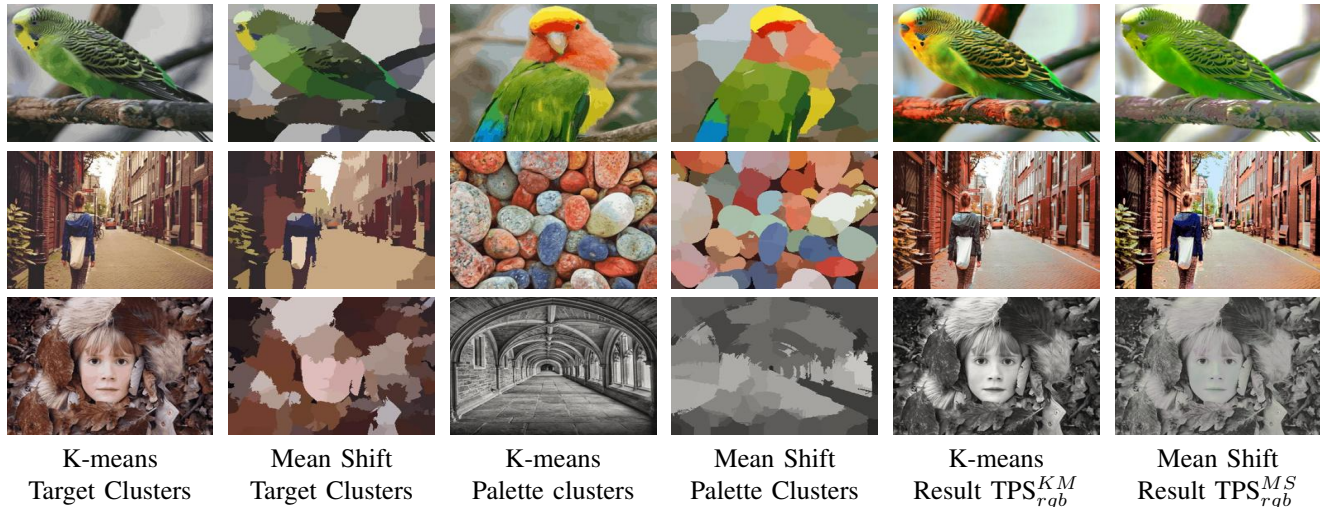


Fig. 4. Comparison between K-means clustering and Mean Shift clustering when setting the Gaussian centres  $\{\mu^{(t)}\}$  of  $p_t$  and  $p_p$ . Columns 1 to 4 show the target and palette images recoloured with the  $K$  cluster centres found using either K-means or Mean Shift. Columns 5 and 6 shows the results obtained by  $\text{TPS}_{rgb}$  using the clusters determined by each algorithm.

between them according to this analysis. Similarly, for images with different content we compared  $\text{TPS}_{rgb}$  and Pitié, the results of which can be seen in Table VIII. In this case both methods were chosen an equal number of times, indicating that there is no perceivable difference between  $\text{TPS}_{rgb}$  and Pitié.

Similar Content $P \simeq T$			
Method	Votes	Prop	CI on Prop
Bonneel	38	0.126	(0.089, 0.164)
Pitié	63	0.210	(0.164, 0.256)
PMLS	98	0.327	(0.274, 0.380)
$\text{TPS}_{rgb}^{Corr}$	101	0.337	(0.283, 0.390)
Different Content $P \neq T$			
Method	Votes	Prop	CI on Prop
Bonneel	163	0.214	(0.185, 0.244)
Pitié	211	0.278	(0.246, 0.310)
Ferradans	152	0.20	(0.172, 0.228)
$\text{TPS}_{rgb}^{KM}$	234	0.308	(0.275, 0.341)

TABLE VII

NUMBER OF VOTES GIVEN TO EACH METHOD BY PARTICIPANTS IN OUR FIRST PERCEPTUAL STUDY (BEST INDICATED IN RED, SECOND BEST IN GREEN, THIRD BEST IN BLUE), THEIR CORRESPONDING PROPORTION AND CONFIDENCE INTERVAL.

#### D. Computation Time

It is important to provide timely feedback for artists and amateurs alike when recolouring image and video materials. The recolouring step is highly parallelisable, allowing the recolouring of video content at a high speed. In terms of computation, our algorithm is split into three parts: the clustering step, the estimation step of  $\theta$  and the recolouring step  $x \rightarrow \phi(x, \theta)$ . As K-means can be quite a time consuming clustering technique, we investigated some fast quantisation methods including those provided by Matlab and the GNU Image Manipulation Program (GIMP)[43]. We found that using

Similar Content $P \simeq T$					
Method	Votes	Prop	CI on Prop	Score	CI on score
PMLS	134	0.447	(0.390, 0.503)	-0.190	(0.303, -0.076)
$\text{TPS}_{rgb}^{Corr}$	166	0.553	(0.497, 0.610)	0.190	(0.077, 0.303)
Different Content $P \neq T$					
Method	Votes	Prop	CI on Prop	Score	CI on score
Pitié	380	0.5	(0.443, 0.557)	0	(-0.1132, 0.1132)
$\text{TPS}_{rgb}^{KM}$	380	0.5	(0.443, 0.557)	0	(-0.1132, 0.1132)

TABLE VIII

NUMBER OF VOTES GIVEN TO EACH METHOD BY PARTICIPANTS IN OUR SECOND PERCEPTUAL STUDY (BEST INDICATED IN RED, SECOND BEST IN GREEN, THIRD BEST IN BLUE), CORRESPONDING PROPORTION AND CONFIDENCE INTERVAL, THURSTONE SCORE AND ASSOCIATED CONFIDENCE INTERVAL.

Matlab's minimum variance quantisation method (MVQ)[44] provided almost identical results to K-means as well as being much faster and could be used as an alternative to K-means to speed up the clustering step (Table IX). A comparison between these techniques and K-means can be seen in Figure 6.

The estimation step takes approximately 6 seconds using non optimised code. Once  $\theta$  is estimated however, it can then be used to recolour an image of any size, or be applied to recolour a video clip. It can also be stored for later usage (see paragraph V-A).

The recolouring step on the other hand is highly parallelisable and can be applied independently to each pixel. The time taken to recolour a HD image for each type of radial basis function is given in Table IX. In our implementation we used OpenMP within a Matlab mex file to parallelise this step on 8 CPU threads. All times are computed on a 2.93GHz Intel CPU with 3GB of RAM with 4 cores and 8 logical processors. In comparison, the GPU implementation of PMLS takes 4.5 seconds to recolour a 1 million pixel image using an nVIDIA Quadro 4000 as reported in [7], which is 9 times slower than our implementation with TPS. Similarly, Bonneel et al. report

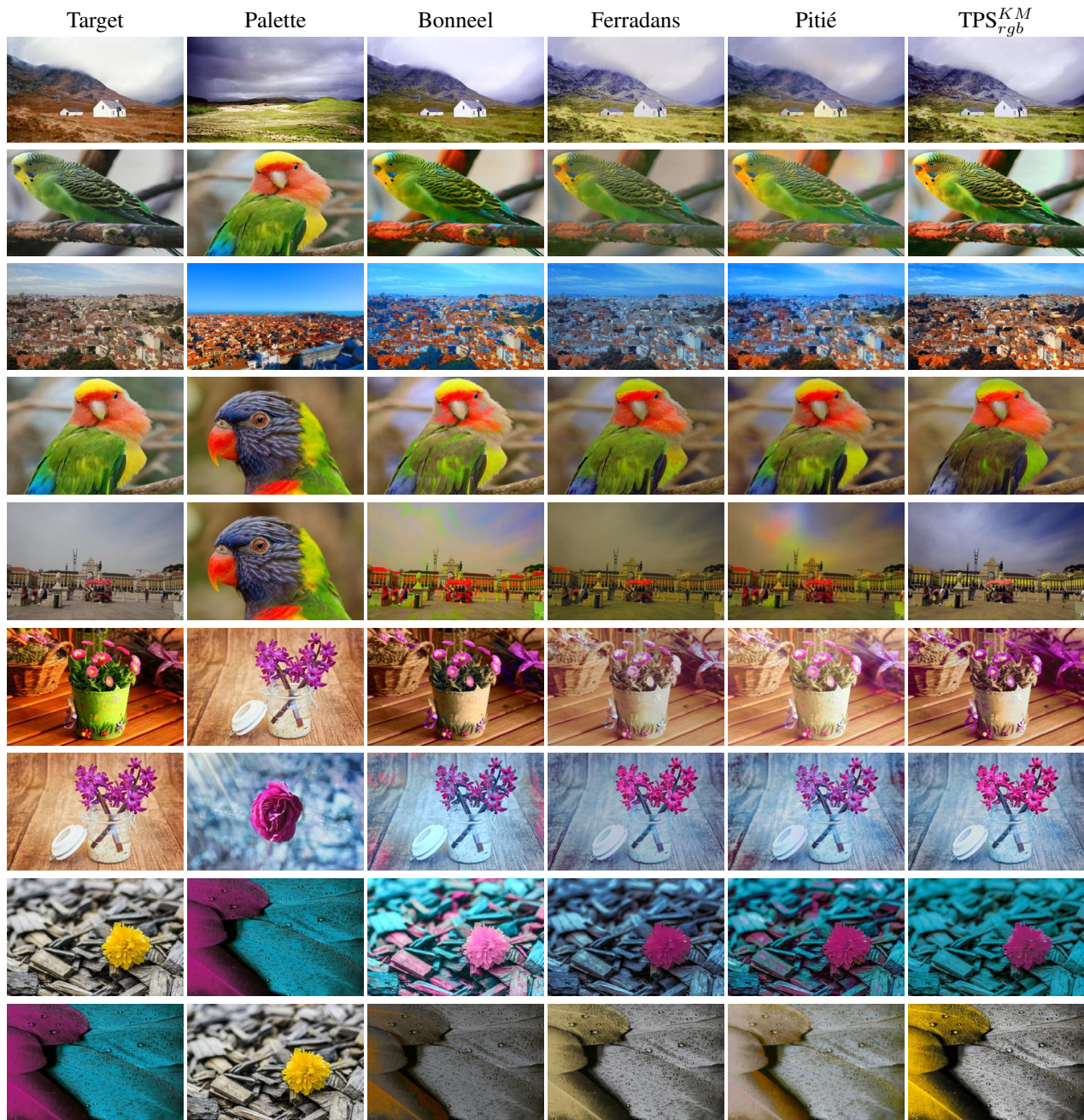


Fig. 5. Some results on images with different content which were presented to participants in the user study.

a time of approximately 3 minutes to recolour 108 frames of a HD segmented video on an 8 core machine with their algorithm [45]. In comparison, our algorithm would take less than 2 minutes using TPS in the same situation.

It can also be applied to each pixel in parallel and a GPU implementation would allow videos to be recoloured extremely quickly.

## V. USABILITY FOR RECOLOURING

The estimated parametric transfer function computed by our algorithms can be stored and combined easily with other transfer functions computed using various colour palettes for the creation of visual effects (cf. Section V-A). Existing

postprocessing can also be used to further improve the quality of the results (Section V-B).

### A. Mixing colour palettes

Once estimated, the parametric transformation can be easily applied to video content [2], [19]. Interpolating between two parametric transformations  $\hat{\theta}^{(1)}$  and  $\hat{\theta}^{(2)}$  can also be used to create interesting effects in images.

The interpolating weight can also vary over time  $\gamma(t) \in [0; 1]$  to create dissolve effects between colour palettes in videos, and can be applied as follows to each colour pixel

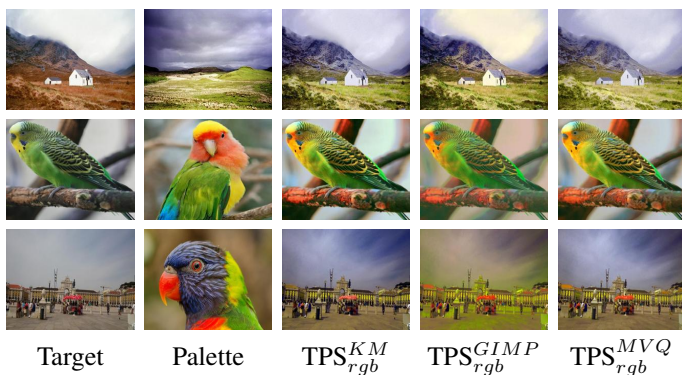


Fig. 6. Comparison between the results obtained using the K-means clustering technique and two faster quantisation techniques.  $TPS_{rgb}^{GIMP}$  are the results obtained when the target and palette images have been clustered using GIMP’s quantisation method (the median cut algorithm).  $TPS_{rgb}^{MVQ}$  are the results obtained when Matlab’s minimum variance quantisation algorithm is used to cluster the images.  $TPS_{rgb}^{MVQ}$  gives results that are very similar to  $TPS_{rgb}^{KM}$ .

Clustering	
Method	Time
K-means	10.4s
Mean Shift	3.2s
MVQ	0.005s
Estimating $\hat{\theta}$	
K	Time
K = 50	6s
Recolouring	
RBF name	Time
TPS	1.04s
Gaussian	3.31s
Inverse Multiquadric	3.16s
Inverse Quadric	2.74s

TABLE IX

COMPUTATION TIMES IN SECONDS FOR EACH STEP OF OUR ALGORITHM FOR A HD (1080 × 1920) IMAGE WITH OVER 2 MILLION PIXELS. (FOR THE CLUSTERING STEP, THE IMAGES WERE FIRST DOWNSAMPLED TO 300 × 350 PIXELS TO REDUCE COMPUTATION TIME).

$x$  at pixel spatial location  $p = (p_1, p_2)$  in the sequence at time  $t$  [2]:

$$x(p, t) \rightarrow \phi \left( x, \gamma(t) \hat{\theta}^{(1)} + (1 - \gamma(t)) \hat{\theta}^{(2)} \right). \quad (19)$$

We extend this idea further using interpolation weights that vary spatially, as well as in the temporal domain, where pixels are recoloured as follows:

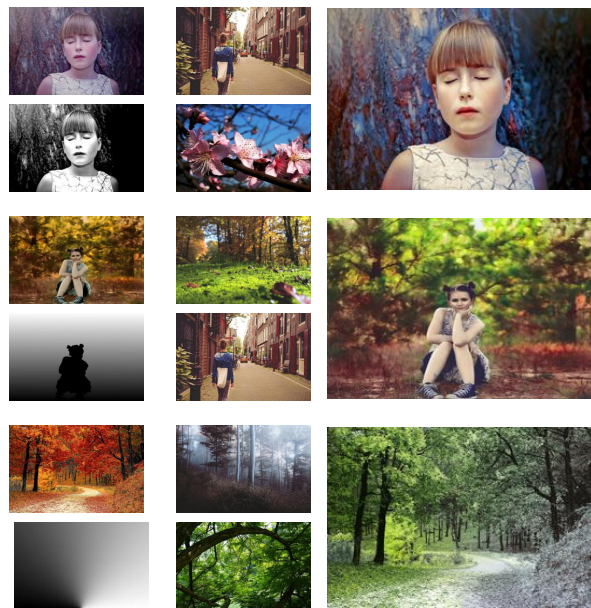
$$x(p, t) \rightarrow \phi \left( x, \gamma(p, t) \hat{\theta}^{(1)} + (1 - \gamma(p, t)) \hat{\theta}^{(2)} \right) \quad (20)$$

$\gamma(p, t)$  is a dynamic greyscale mask with values between 0 and 1. Figure 7 presents some examples of results on images<sup>7</sup>. Moreover these effects can be extended to mixing more than 2 transformations (or palettes). A simpler interpolation between the identity transformation  $\theta^{(Id)}$  and an estimated transformation  $\hat{\theta}$  with a selected colour palette can also be created:

$$x(p, t) \rightarrow \phi \left( x, \gamma(t) \hat{\theta}^{(Id)} + (1 - \gamma(t)) \hat{\theta} \right) \quad (21)$$

This gives the user the flexibility to transition smoothly from one colour mood to another.

<sup>7</sup>Supplementary results for videos are provided by the authors.



Target & Mask Palettes 1 & 2 Results  $TPS_{rgb}^{KM}$

Fig. 7. Mask  $\gamma(p)$  is used to vary the recolouring spatially. The results images were generated using the target and mask (column 1) and two palette images (column 2). Pixels in the target image whose corresponding pixel in the grey scale mask is white have been recoloured using palette 1 (top), and those whose corresponding pixel is black have been recoloured using palette 2 (bottom). The remaining pixels have been recoloured using an interpolation between the two transformations. For each pixel this interpolation is determined by the value of its corresponding pixel in the grey scale mask. Images shown are public domain images sourced from pixabay.com.

## B. Post-processing

While our approach produces excellent results in general, rare saturation artifacts can occur when many colours in the palette image lie close to the boundary of the colour space. As we do not constrain the transformed colours to lie within a specific range, some colours can potentially get transformed outside of the colour space. Currently we clamp the colour values so that they are within the desired range. Recently Oliveira et al. [25] proposed using truncated Gaussians which could be implemented in future to overcome this problem. Additionally, a post-processing step could be added to our pipeline when needed, to constrain the smoothness of the gradient field of the recoloured image to be similar to the gradient field of the target image as proposed by [9] (c.f. Figure 8).

## VI. CONCLUSION

We have presented a new framework for colour transfer that is able to take into account correspondences when these are available. Our algorithms compete very well with current state of the art approaches since no statistical differences can be measured using metrics such as SSIM, PSNR and CID with the current top techniques, and visual inspection of our results show that our algorithms are more immune to occasional artifacts that can be created in the gradient field of the recoloured image. Our parametric formulation of the transfer function allows for fast recolouring of images and

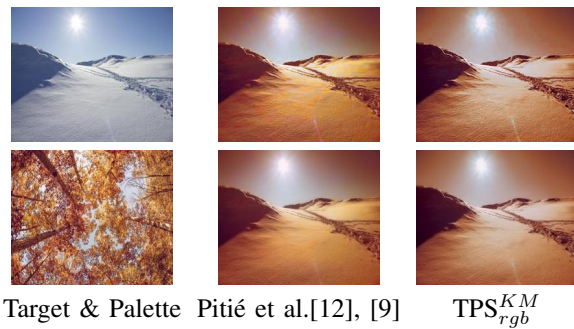


Fig. 8. Example of quantisation errors enhanced by our transfer method (e.g. in the sky) as the gradient becomes stretched to match the colours in the palette image (row 1, col 3). The gradient smoothing step proposed by Pitié et al. [9] as an improvement from their earlier method without post processing [12] could be used in our pipeline to remove artifacts, although in general this can reduce the sharpness of the image which is undesirable. Column 2: Pitié et al. [12] (before smoothing) and [9] (after smoothing); Column 3:  $TPS_{rgb}^{KM}$  (before smoothing) and  $TPS_{rgb}^{KM}$  (after smoothing).

videos. Moreover transfer functions can be stored and easily combined and interpolated for creating visual effects. Future work will investigate techniques to capture users' preferences by learning from exemplar transfer functions [46].

#### ACKNOWLEDGEMENTS

This work has been supported by a Ussher scholarship from Trinity College Dublin (Ireland), and partially supported by EU FP7-PEOPLE-2013- IAPP GRAISearch grant (612334).

#### REFERENCES

- [1] M. Grogan, M. Prasad, and R. Dahyot, "L2 registration for colour transfer," in *Proceedings of the 23rd European Signal Processing Conference (EUSIPCO)*, ser. EUSIPCO '15, Nice, France, 2015, pp. 2366–2370.
- [2] M. Grogan and R. Dahyot, "L2 registration for colour transfer in videos," in *Proceedings of the 12th European Conference on Visual Media Production*, ser. CVMP '15. New York, NY, USA: ACM, 2015, pp. 16:1–16:1.
- [3] H. S. Faridul, T. Pouli, C. Chamaret, J. Stauder, A. Tremeau, and E. Reinhard, "A Survey of Color Mapping and its Applications," in *Eurographics 2014 - State of the Art Reports*, S. Lefebvre and M. Spagnuolo, Eds. The Eurographics Association, 2014.
- [4] V. Naranjo and A. Albiol, "Flicker reduction in old films," in *International Conference on Image Processing (ICIP)*, 2000.
- [5] E. Reinhard, M. Adhikmin, B. Gooch, and P. Shirley, "Color transfer between images," *Computer Graphics and Applications, IEEE*, vol. 21, no. 5, pp. 34–41, Sep 2001.
- [6] N. Bonneel, J. Rabin, G. Peyr, and H. Pfister, "Sliced and radon wasserstein barycenters of measures," *Journal of Mathematical Imaging and Vision*, vol. 51, no. 1, pp. 22–45, 2015.
- [7] Y. Hwang, J.-Y. Lee, I. S. Kweon, and S. J. Kim, "Color transfer using probabilistic moving least squares," in *Computer Vision and Pattern Recognition (CVPR), 2014 IEEE Conference on*, June 2014, pp. 3342–3349.
- [8] S. Ferradans, N. Papadakis, J. Rabin, G. Peyr, and J.-F. Aujol, "Regularized discrete optimal transport," in *Scale Space and Variational Methods in Computer Vision*, ser. Lecture Notes in Computer Science, A. Kuijper, K. Bredies, T. Pock, and H. Bischof, Eds. Springer Berlin Heidelberg, 2013, vol. 7893, pp. 428–439.
- [9] F. Pitié, A. C. Kokaram, and R. Dahyot, "Automated colour grading using colour distribution transfer," *Comput. Vis. Image Underst.*, vol. 107, no. 1–2, pp. 123–137, Jul. 2007.
- [10] C. Villani, *Optimal transport : old and new*, ser. Grundlehren der mathematischen Wissenschaften. Berlin: Springer, 2009.
- [11] —, *Topics in Optimal Transportation*. American Mathematical Society, 2003, vol. 58.
- [12] F. Pitié, A. Kokaram, and R. Dahyot, "N-dimensional probability density function transfer and its application to color transfer," in *Computer Vision, 2005. ICCV 2005. Tenth IEEE International Conference on*, vol. 2, Oct 2005, pp. 1434–1439 Vol. 2.
- [13] L. Neumann and A. Neumann, "Color style transfer techniques using hue, lightness and saturation histogram matching," in *Proceedings of the First Eurographics Conference on Computational Aesthetics in Graphics, Visualization and Imaging*, ser. Computational Aesthetics'05. Aire-la-Ville, Switzerland, Switzerland: Eurographics Association, 2005, pp. 111–122.
- [14] N. Papadakis, E. Provenzi, and V. Caselles, "A variational model for histogram transfer of color images," *Image Processing, IEEE Transactions on*, vol. 20, no. 6, pp. 1682–1695, June 2011.
- [15] T. Pouli and E. Reinhard, "Progressive color transfer for images of arbitrary dynamic range," *Computers & Graphics*, vol. 35, no. 1, pp. 67 – 80, 2011, extended Papers from Non-Photorealistic Animation and Rendering (NPAR) 2010.
- [16] D. Freedman and P. Kisilev, "Object-to-object color transfer: Optimal flows and smp transformations," in *Computer Vision and Pattern Recognition (CVPR), 2010 IEEE Conference on*, June 2010, pp. 287–294.
- [17] X. Xiao and L. Ma, "Gradient-preserving color transfer," *Computer Graphics Forum*, vol. 28, no. 7, pp. 1879–1886, 2009.
- [18] J. Rabin, J. Delon, and Y. Gousseau, "Removing artefacts from color and contrast modifications," *Image Processing, IEEE Transactions on*, vol. 20, no. 11, pp. 3073–3085, Nov 2011.
- [19] O. Frigo, N. Sabater, V. Demoulin, and P. Hellier, "Optimal transportation for example-guided color transfer," in *Computer Vision – ACCV 2014*, ser. Lecture Notes in Computer Science, D. Cremers, I. Reid, H. Saito, and M.-H. Yang, Eds. Springer International Publishing, 2015, vol. 9005, pp. 655–670.
- [20] K. Jeong and C. Jaynes, "Object matching in disjoint cameras using a color transfer approach," *Machine Vision and Applications*, vol. 19, no. 5, pp. 443–455, 2007.
- [21] Y. Xiang, B. Zou, and H. Li, "Selective color transfer with multi-source images," *Pattern Recognition Letters*, vol. 30, no. 7, pp. 682 – 689, 2009.
- [22] D. Comaniciu and P. Meer, "Mean shift: a robust approach toward feature space analysis," *Pattern Analysis and Machine Intelligence, IEEE Transactions on*, vol. 24, no. 5, pp. 603–619, May 2002.
- [23] S. Xu, Y. Zhang, S. Zhang, and X. Ye, "Uniform color transfer," in *IEEE International Conference on Image Processing 2005*, vol. 3, Sept 2005, pp. III–940–3.
- [24] Y.-W. Tai, J. Jia, and C.-K. Tang, "Local color transfer via probabilistic segmentation by expectation-maximization," in *2005 IEEE Computer Society Conference on Computer Vision and Pattern Recognition (CVPR'05)*, vol. 1, June 2005, pp. 747–754 vol. 1.
- [25] M. Oliveira, A. Sappa, and V. Santos, "A probabilistic approach for color correction in image mosaicking applications," *Image Processing, IEEE Transactions on*, vol. 24, no. 2, pp. 508–523, Feb 2015.
- [26] Y. HaCohen, E. Shechtman, D. B. Goldman, and D. Lischinski, "Non-rigid dense correspondence with applications for image enhancement," *ACM Trans. Graph.*, vol. 30, no. 4, pp. 70:1–70:10, Jul. 2011.
- [27] B. Jian and B. Vemuri, "Robust point set registration using gaussian mixture models," *Pattern Analysis and Machine Intelligence, IEEE Transactions on*, vol. 33, no. 8, pp. 1633–1645, Aug 2011.
- [28] C. Arellano and R. Dahyot, "Robust ellipse detection with gaussian mixture models," *Pattern Recognition*, 2016.
- [29] F. Escolano, P. Suau, and B. Bonev, *Information theory in Computer Vision and Pattern Recognition*. Springer, 2009.
- [30] D. W. Scott, "Parametric statistical modeling by minimum integrated square error," *Technometrics*, vol. 43, no. 3, pp. pp. 274–285, 2001.
- [31] B. Jian and B. C. Vemuri, "A robust algorithm for point set registration using mixture of gaussians," in *International Conference on Computer Vision (2005)*, 2005.
- [32] C. Arellano and R. Dahyot, "Shape model fitting algorithm without point correspondence," in *20th European Signal Processing Conference (Eusipco)*, Bucharest, Romania, August, 27–31 2012, pp. 934–938.
- [33] —, "Robust bayesian fitting of 3d morphable model," in *Proceedings of the 10th European Conference on Visual Media Production*, ser. CVMP '13. New York, NY, USA: ACM, 2013, pp. 9:1–9:10.
- [34] S. Belongie, J. Malik, and J. Puzicha, "Shape matching and object recognition using shape contexts," *Pattern Analysis and Machine Intelligence, IEEE Transactions on*, vol. 24, no. 4, pp. 509–522, Apr 2002.
- [35] D. Lowe, "Distinctive image features from scale-invariant keypoints," *International Journal on Computer Vision*, vol. 60, no. 2, p. 91110, 2004.

- [36] J. Ma, J. Zhao, J. Tian, Z. Tu, and A. L. Yuille, "Robust estimation of nonrigid transformation for point set registration," in *IEEE Conference on Computer Vision and Pattern Recognition*, Portland, OR, USA USA, June 23-28 2013.
- [37] F. Pitić and A. Kokaram, "The linear monge-kantorovitch linear (mkl) colour mapping for example-based colour transfer," in *4th European Conference on Visual Media Production*, 2007.
- [38] X. Wu, V. Kumar, J. Ross Quinlan, J. Ghosh, Q. Yang, H. Motoda, G. J. McLachlan, A. Ng, B. Liu, P. S. Yu, Z.-H. Zhou, M. Steinbach, D. J. Hand, and D. Steinberg, "Top 10 algorithms in data mining," *Knowl. Inf. Syst.*, vol. 14, no. 1, pp. 1–37, Dec. 2007.
- [39] M. Carreira-Perpinan, "Gaussian mean-shift is an em algorithm," *IEEE Transactions on Pattern Analysis and Machine Intelligence*, vol. 29, no. 5, pp. 767 – 776, May 2007.
- [40] I. Lissner, J. Preiss, P. Urban, M. S. Lichtenauer, and P. Zolliker, "Image-difference prediction: From grayscale to color," *IEEE Transactions on Image Processing*, vol. 22, no. 2, pp. 435–446, Feb 2013.
- [41] H. Hristova, O. Le Meur, R. Cozot, and K. Bouatouch, "Style-aware robust color transfer," in *Proceedings of the Workshop on Computational Aesthetics*, ser. CAE '15. Aire-la-Ville, Switzerland, Switzerland: Eurographics Association, 2015, pp. 67–77.
- [42] J. Morovič, "Color gamut mapping," 2008.
- [43] [Online]. Available: <https://www.gimp.org/>
- [44] [Online]. Available: <https://uk.mathworks.com/help/matlab/ref/rgb2ind.html>
- [45] N. Bonneel, K. Sunkavalli, S. Paris, and H. Pfister, "Example-based video color grading," *ACM Trans. Graph.*, vol. 32, no. 4, pp. 39:1–39:12, Jul. 2013.
- [46] Z. Yan, H. Zhang, B. Wang, S. Paris, and Y. Yu, "Automatic photo adjustment using deep neural networks," *ACM Trans. Graph.*, vol. 35, no. 2, pp. 11:1–11:15, Feb. 2016.